frontiers | Frontiers in Earth Science

TYPE Original Research
PUBLISHED 06 August 2025
DOI 10.3389/feart.2025.1597461

OPEN ACCESS

EDITED BY
Eun Young Lee,
University of Vienna, Austria

REVIEWED BY
Fangbin Liu,
Qilu Normal University, China
Bin Zhang,
Chinese Academy of Geological Sciences Institute of Geology, China

*CORRESPONDENCE
Hongcai Shi,
hcshi@gdou.edu.cn
Hui Xie,
xiehuihaoba@163.com

RECEIVED 21 March 2025
ACCEPTED 21 July 2025
PUBLISHED 06 August 2025

CITATION
Shi H, Xie H, Zhao W, Liu T, Kong D, Bao C and Liu L (2025) Thermal evolution of Cathaysian block along the South China margin since the Late Cretaceous: evidence from low-temperature thermochronology. *Front. Earth Sci.* 13:1597461. doi: 10.3389/feart.2025.1597461

Thermal evolution of Cathaysian block along the South China margin since the Late Cretaceous: evidence from low-temperature thermochronology

Hongcai Shi[1,2]*, Hui Xie[1,2,3]*, Weina Zhao[4], Tangwei Liu[5], Deming Kong[1,2], Chuang Bao[1,2] and Lijie Liu[5]

[1]Key Laboratory of Climate, Resources and Environment in Continental Shelf Sea and Deep Sea of Department of Education of Guangdong Province, Guangdong Ocean University, Zhanjiang, China, [2]Laboratory for Coastal Ocean Variation and Disaster Prediction, College of Ocean and Meteorology, Guangdong Ocean University, Zhanjiang, China, [3]Key Laboratory of Marine Mineral Resources, Ministry of Natural Resources, Guangzhou, China, [4]School of Marine Science and Technology, Northwestern Polytechnical University, Xi'an, China, [5]School of Science, East China University of Technology, Nanchang, China

The Cathaysian Block has undergone complex tectonic transformation since the Mesozoic, with significant topographic and geomorphological changes due to large-scale magmatism, as well as tectonism in the central area. Apatite fission track (AFT) and zircon (U-Th)/He (ZHe) data were used to reveal the tectonic-thermal evolution history of the southeastern margin of the Cathaysian Block in the coastal region during the Late Cretaceous in this paper. Results suggest AFT ages range between 36.3 ± 2.7 Ma and 63.5 ± 6.7 Ma with mean confined track lengths from 12.99 ± 1.54 μm to 13.7 ± 1.54 μm. ZHe ages are ranged from 72.6 ± 4.5 to 113.3 ± 7.0 Ma and concentrated in 90-100 Ma. Thermal history modeling indicated a multi-stage cooling history: (1) Widespread Late Cretaceous to Paleocene cooling across the entire coastal mountain. The Late Cretaceous cooling was coincident with rollback of the subducted paleo-Pacific Plate, which resulted in a negative inversion from compression to extension. (2A) rapid cooling beginning at ~60 Ma and at ~45 Ma, which was interpreted as temporally coinciding with continental rifting along the Cathaysian coastal margin, considered to have signaled the opening of the South China Sea (SCS); and (2B) a subsequent slow cooling stage with a small temperature change at ~50°C–65°C during the Oligocene to middle Miocene, accompanied by migration of the central rift to the marine basin. (3) A final stage of rapid cooling to surface temperature commencing about 18 and 10 Ma since the Miocene in response to multiple-plates interaction caused by the Tibetan Plateau uplift and the collision of the Philippine Block with the Eurasian continent.

KEYWORDS

Cathaysian block, fission track, coastal mountains of SE China, tectono-thermal evolution, (U-Th)/He

1 Introduction

The South China Block (SCB), a major component of SE Asia, comprises the Yangtze block to the NW and the Cathaysian block to the SE (Li et al., 2014). The southern margin of the Cathaysian block has experienced complex tectonic evolution since the Late Mesozoic (Xiao et al., 2024; Li et al., 2014; 2019; Suo et al., 2019; Zhang et al., 2013). Following the Indosinian orogeny, this region developed into an active Andean-type margin dominated by northward subduction of the Paleo-Pacific Plate (Zhou et al., 2006; Li and Li, 2007). During the Cenozoic however, the tectonic regime transitioned progressively from an active to passive continental margin, driven by interaction between the Indo-Australian, Eurasian and Pacific Plates (e.g., Hall, 2012). As a result, the southern SCB margin has recorded multiple episodes of alternating compressional and extensional deformation regimes, accompanied by associated magmatic activity since the Late Mesozoic (e.g., Shi et al., 2022; Shu et al., 2009; Li et al., 2014). The tectonic transition displays distinct spatial variability, with onshore basins (e.g., Nanxiong and Sanshui) exhibiting complex inversion structures (Zhao et al., 2025), whereas offshore domains maintained continuous sedimentation during South China Sea spreading (32–16 Ma; Oligocene-Early Miocene) but show significant spatiotemporal variations across sub-basins (e.g., Barckhausen et al., 2014). There are still significant disagreements on the Cenozoic tectono-thermal history of the onshore regions, especially in Guangdong Province, despite the fact that this region has seen a large number of structural geological investigations. Therefore, accurate determination of the thermochronological record and spatial patterns of major tectonic events (e.g., Yanshanian deformation, SCS expansion) is fundamental for deciphering the geodynamic evolution of this margin.

Mesozoic granitic rocks exposed on the surface in the coastal mountains contain abundant information about the formation and evolution of the continental crust, and is an instrument for understanding the dynamic background of the deep-seated continental lithosphere. However, the low-temperature thermochronology, including fission track (FT) and (U-Th)/He methods, are widely used to reveal the cooling history of continental margin and orogenic belts (e.g., Shi et al., 2016; Tao et al., 2017; Liu et al., 2022; 2024). Although many low-temperature thermochronological datasets of magmatic rock in the Cathaysian block have been reported (Figure 1) (e.g., Li and Zou, 2017; Li et al., 2005; Shi et al., 2011; 2022; Tao et al., 2017, Tao et al., 2019; Yan et al., 2009; Zhang, 2007), the timing and mechanisms of its origin remain debated (Tao et al., 2017; Tao et al., 2019; Wang et al., 2020a; Yan et al., 2009). To better reconstruct a more comprehensive thermal history and reveal the evolution of the exposed coastal mountains in the Cathaysian block, we report multi-system low-temperature thermochronology data that constrain the thermal history of the southern Cathaysian block coastal region granites in this study. The results provide new insights into thermal history and contribute to delineate the timing of tectonic transition and decipher the geodynamic evolutionary processes of the southern Cathaysian block since the late Mesozoic.

2 Geological setting

2.1 Regional geology and tectonic evolution

The South China Block is located in the south of the North China Block, separated from it by the Qinling-Dabie orogenic belt, and in the west of the Qinghai-Tibetan Plateau, separated from the Indochina Block to the southwest by the Qinghai-Tibet Plateau and from the Pacific Plate by the South China Sea (Figure 1A) (Li et al., 2013; 2014). The Mesozoic basin-range tectonic province of the Cathaysian Block has experienced multiphase tectonic superposition and deformation, with concomitant transitions from active to passive continental margin regimes (Suo et al., 2019). Four major stages of regional tectono-thermal evolution since the Paleozoic have been identified as (1) the Paleozoic (Caledonian) orogeny, which resulted in an angular unconformity between the Lower and Middle Devonian strata; (2) the late Permian–Triassic (Indosinian) orogeny resulted in prominent crustal thickening and shortening and created an ~1,300 km wide NE-NNE trending intracontinental orogenic belt (Li and Li, 2007; Li et al., 2014), identified by folded pre-Triassic strata and a regional unconformity; and (3) Middle Jurassic and Cretaceous (early/late Yanshanian) magmatism and extension (Li et al., 2016; Wang et al., 2020b; 2013; Zheng et al., 2019) followed by (4) localized Paleogene continental rifting and multi-plate activity since the late Eocene (Suo et al., 2019; Wang et al., 2020a). Because of the crustal extension during the Yanshanian orogeny, the basin-range tectonic province was formed due to rollback of the subducted paleo-Pacific Plate (e.g., Li and Li, 2007; Tian and Di, 2024; Yan et al., 2024). Triassic rocks and structures were rejuvenated in the Yanshanian orogeny. As a result of the long-lasting extension and rifting since the Cretaceous, the crust has gradually thinned from 28 to 26 km in the continental margin of South China, and from 15 to 8 km in the South China Sea (Tao et al., 2017; Zhang and Wang, 2007).

Two fault systems trending NE-NNE and NW-W were developed in the Cathaysian Block (Wang et al., 2020b). The Cathaysian Block is structurally dominated by a NE-NNE-trending fault system, with predominant NW- or SE-dipping orientations. This system comprises major faults such as the Changle-Nan'ao (CNF), Zhenghe-Dapu (ZDF), Xinfeng-Enping (XEF), Heyuan (HF), and Sihui-Wuchuan (SWF) faults (Figure 1B; Li et al., 2014). These faults typically truncate Devonian to Jurassic stratigraphic sequences and effectively partition the block into three distinct tectonic domains: (1) the southeastern coastal magmatic belt, (2) the central Cathaysian fold-thrust belt, and (3) the northwestern Cathaysian interior belt.

In terms of the sedimentology of the region, after marine deposition ended in the late Paleozoic many sets of continental deposits were developed (Tao et al., 2017). The first is the late Triassic-Middle Jurassic strata composed of sandstones and shales with claystones and coal seams, overlain by Cretaceous strata which are mainly red quartz sandy conglomerate and tuff, then late Eocene sandstones and sparse Quaternary sediment rocks (GBGMR, 1988), all with unconformable contact. Middle Triassic strata are missing in the Cathaysian Block, resulting in an unconformable contact between late and Lower Triassic strata. Eocene sandstone directly overlies Cretaceous strata, which unconformably overlies Middle

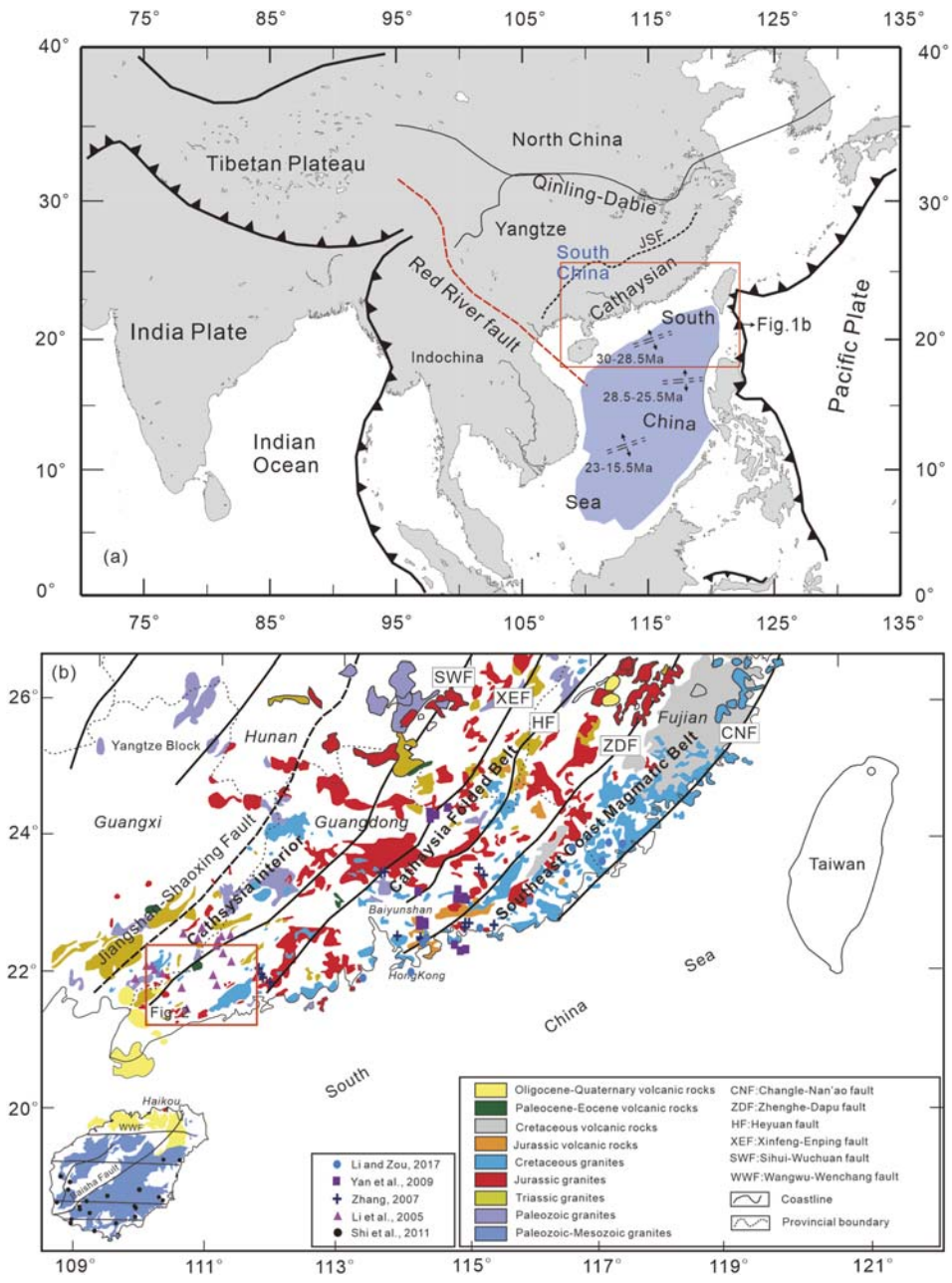

FIGURE 1
(A) Sketch of regional tectonics in SE Asia and location of study area; **(B)** Mesozoic and Cenozoic plutons at southern margin of the Coastal mountains, showing sampling locations and main tectonic units (modified from Shi et al., 2011; Tao et al., 2017).

Jurassic strata, with late Jurassic rocks missing (GBGMR, 1988). The sparse Quaternary strata sit unconformably on Eocene or Cretaceous sediments (GBGMR, 1988).

2.2 Magmatic rocks and magmatism

South China is a large area of granites rarely seen in the world. Granites of different ages are exposed, especially Mesozoic granites, with an outcrop area of 218,090 km^2, accounting for 28.3% of the total land surface in the region (Zhou and Li, 2000; Zhou et al., 2006). The dates of the granite formation is mainly concentrated in the Lower to Upper Triassic (251–205 Ma), the Jurassic (~190–142 Ma) and the Lower to Upper Cretaceous (~137–66 Ma).

Lower Triassic granites (zircon U-Pb: 251–234 Ma) occur sporadically as plutons along the coastal margin of SE China; Late Triassic plutons (210–230 Ma) are found only in the interior of the central Cathaysian Block (Meng et al., 2012; Peng et al., 2006; Yue et al., 2024; Tian and Di, 2025) with gneissic/mylonitized structures (Zhou et al., 2006), which reveals a tendency to gradually migrate northwestward of the site of magmatism

(Li and Li, 2007). Formation of the Indosinian (T_1-T_3) S-type granites rich in aluminum was influenced by collisional compression (Zhou et al., 2006).

The onset of the Yanshanian orogeny, the third tectono-thermal event (Tao et al., 2019), was an episode of fresh magmatism commencing early in the Jurassic as indicated by A-type granites emplaced at 189 ± 3 Ma and contemporaneous mafic intrusives and rhyolites (Li and Li, 2007; Meng et al., 2012; Yu et al., 2010; Zhou et al., 2006) accompanied by doming structures and an extensional basin (Guo et al., 2021; Li et al., 2014). Middle to Late Jurassic granitoids and volcanic rocks are mostly concentrated west of the ZDF in the interior of the Cathaysian Block and having a narrow age range from 180 to 170 Ma. The Jurassic volcanic rock is considered to indicate a rifts origin (Zhou et al., 2006).

Cretaceous magmatic rocks between ca. 137 and 66 Ma include A/I-type granitoids, adakitic rocks and volcanics composed of rhyolite, lava and basalt tuff, including a Lower Cretaceous (K_1) assemblage mostly related to active continental margin magmatism, and Late Cretaceous (K_2) subalkaline basalt exposed in contemporaneous red conglomerate of back-arc extensional basins (Zhou et al., 2006), which are separated by the regional unconformity dating from 120 to 115 Ma (Li et al., 2014). There are obvious differences between the Indosinian (T_1-T_3) and Early Yanshanian (J_2-J_3) rocks in spatiotemporal distribution, rock geochemistry and assemblage. The vast Yanshanian magmatic belts are interpreted to be correlated with the northwestward subduction of the paleo-Pacific Plate (Zhou et al., 2006).

3 Sampling strategy and experimental methods

3.1 Sampling strategy and information

To quantify the magnitude and timing of exhumation resulted from extension due to the foundering and rollback of the subducted paleo-plate and subsequent cooling events (Li et al., 2014), 12 fresh granitoid samples (weathering rind <2 cm thick) were collected from three NW-SE-trending cross sections (100–300 km each), which cut through the principal tectonic domains of the SE China coastal belt and intersect the full suite of nine Cretaceous intrusive bodies (Table 1; Figures 2, 3). The geographic locations and elevations of each sample were determined by a hand-held GPS. The lithology refers to the mineral composition identification and topographic and geological map.

The lithologies of samples are granite/granitic rocks or other intrusive rocks according to the QAPF modal diagram (Figure 4). Certain rock samples displayed distinct mineral alignment or alteration features, e.g., SW02, YF02 and XY01, suggesting that some of them underwent the dynamic metamorphism in the later tectonic evolution. In the paper, three plutons were selected to conduct a comprehensive petrologic description. The Yunfu pluton is composed of quartz-rich granitoid. The sampled rocks consisted mainly of fine-grained quartz (~40–50%), plagioclase (~20–35%), biotite (~10–15%), muscovite (1%–5%) and small amounts of accessory minerals (Figure 4b). The Taishan pluton was fine-grained granodiorite. The common mineral assemblage was quartz (~35%), plagioclase (~43%), muscovite (~10%), and minor amounts of microclinic feldspar (4%), perthite (5%), magnetite (1%) and zircon (1%) (Figure 4c). The Yangxi-Dianbai pluton quartez-rich granitoid and/or tonalite was dominated by quartz (30%–40%), plagioclase (30%–40%) with sericitization at the grain margins (Figure 4a), K-feldspar (20%–30%) and biotite (5%–10%) containing zircon and apatite. Detailed information of sampled rocks is presented in Table 1.

3.2 Analytical methods

Apatite and zircon crystals were separated by traditional/standard crushing, sieving, electromagnetic and heavy liquid mineral separation techniques and euhedral to subhedral grains were selected for AFT and ZHe analyses. All the thermochronology analyses were carried out at the University of Melbourne, basically adopting the procedures described by Gleadow et al. (2015). All ages are "model" ages determined with a range factor (R_s) of 7.17 μm and were directly comparable to ages using the traditional external detector method (Gleadow and Duddy, 1981). To increase the number of measurable confined fission tracks, ^{252}Cf irradiation was applied to the AFT analyses. The confined fission track lengths were corrected using a refractive index of 1.634. RadialPlotter software version 9.5 was used to determine the central ages as well as age components (Vermeesch, 2009).

Single-grain ZHe ages were obtained from three to four zircon crystals per sample, and the final age was calculated as a weighted mean incorporating analytical uncertainties, following the approach of Gleadow et al. (2015). In this paper, U and Th were analyzed by ICP-MS combined with the ^{233}Th and ^{229}U spikes. The ZHe ages were calculated and adjusted for alpha particle emission by F_T correction (Farley et al., 1996) based on the grain dimensions. The weighted mean age was calculated within 2σ standard error using Isoplot software version 4.0 (Ludwig, 1991).

4 Results and interpretation

4.1 Apatite fission track (AFT) ages

The AFT results for 11 granitic rock samples from the Cathaysian coastal mountains (Mainly distributed in western Guangdong Province) with ± 1σ error are given in Table 2 and indicated in Figure 3. Eight sample yielded statistically coherent Cenozoic central ages ranging between 36 ± 2.7 and 63 ± 6.7 Ma,with three samples excluded due to insufficient single-grain counts (apatite grain <20 confined tracks per sample). Among the eight samples, seven yielded Eocene cooling ages (ranging from 36 ± 2.7 to 51 ± 3.4 Ma), while a single sample (YF02) preserved an older Paleocene age (64 ± 6.7 Ma) which was collected from the northernmost part of the study area (maximum elevation ~ 350 m). All these were clearly younger than their corresponding crystallization ages (Tables 1, 2). Furthermore, the samples display a general unimodal original track length distribution with mean confined track lengths varying from ~12.99 ± 1.54 to 13.7 ± 1.54 μm (Table 2). This suggests that they might have cooled through the partial annealing zone (PAZ) monotonously at intermediate cooling rate during the Paleogene. Sample YF02 exhibits the oldest fission track age, with the shortest

TABLE 1 Sample data from Cathaysian coastal mountain belts, SE China Note: Crystallization age after Zhou et al. (2006).

No.	Sample ID	Longitude E (°)	Latitude N (°)	Elv.(m)	Lithos	Crystallization age (Ma)
1	QP01	109°54′20″	21°38′34″	51	Granite	180–142 Ma
2	SW02	109°45′56″	21°53′46″	73	Quartz-rich granitoid	180–142 Ma
3	SH02	109°29′34″	22°17′16″	200	Monzogranite	251–205 Ma
4	YL02	110°15′58″	22°47′21″	125	Granite	180–142 Ma
5	LW01	110°44′04″	22°48′56″	300	Granite	180–142 Ma
6	MM02	110°46′53″	22°30′19″	293	Monzogranite	>251 Ma
7	XY01	110°54′03″	22°18′57″	180	Granitic gneiss	180–142 Ma
8	YF02	112°04′11″	22°53′37″	350	Quartz-rich granitoid	180–142 Ma
9	YX01	111°32′28″	21°49′11″	15	Granite	180–142 Ma
10	YX02	111°31′33″	21°38′59″	55	Quartz-rich granitoid/Tonalite	180–142 Ma
11	DB01	111°18′50″	21°31′06″	6	Monzogranite	180–142 Ma n
12	TS01	112°53′17″	22°13′24″	30	Granodiorite	180–142 Ma n

Note: the crystallization age refers to Zhou et al. (2006) and lithology of some samples was determined according to the QAPF, modal diagram.

mean track length but a large standard deviation value of 12.9 ± 1.8 μm.

Three additional samples (QP01, SW02, YL02) mentioned above yielded Miocene ages (10 ± 0.5 to 15 ± 1.1 Ma), with mean confined track lengths between 13.0 ± 2.2 and 13.8 ± 1.4 μm, though their limited grain counts (<20 grains per aliquot) preclude robust statistical analysis. However, apatite fission track single-grain age distributions reveal multiple discrete age peaks in certain samples (Figure 5), and not all samples passed the χ^2 test (<5%) and their AFT central ages are obviously much younger than their crystallization ones. The failure to pass the chi-square test (p <5%) is primarily attributed to small apatite crystal sizes and insufficient spontaneous fission track counts per grain (typically <15-20 tracks), resulting in statistically significant inter-grain age variability that exceeds the expected Poisson distribution.

4.2 Zircon (U-Th)/He (ZHe) ages

The four samples listed in Table 3 yielded Eocone to Late Cretaceous zircon (U-Th)/He (ZHe) ages ranging from 47 ± 2.9 to 113 ± 7.0 Ma (1σ), with mean weighed age 86 ± 6.2 to 103 ± 6.4 Ma (2σ), which demonstrate a good grain-to-grain reproducibility. These cooling ages are systematically younger than their corresponding crystallization ages. Some zircon grains (e.g., TS01-2, YX02-2) exhibit anomalously high eU concentrations, with their corresponding ZHe ages showing a negative correlation with eU values (Figure 6). The negative age-eU correlation reflects radiation damage effects on He retention, particularly in grains with eU >500 ppm (Anderson et al., 2017). Radiation damage from U/Th decay increases He diffusion in zircon, causing age rejuvenation in high-eU grains (eU >2,500 ppm) (Guenthner et al., 2013). ZHe data also show Eocene-reset ages in high-damage zircons (TS01-3), contrasting with Cretaceous cooling signals retained in low-eU grains (eU <2,500 ppm) (Table 3). Therefore, grains (eU <2,500) with ages ranging from 73 ± 4.5 to113 ± 7.0 Ma (1σ) are preferentially selected, as this range typically yields the most stable (U-Th)/He age records (e.g., Guenthner et al., 2013). While these grains provide important constraints on maximum paleo-temperatures (following Guenthner et al., 2013), their ages should be interpreted as minimum estimates for cooling through the partial retention zone. This suggests that post-Late Cretaceous samples did not experience temperatures exceeding 160°C (Guenthner et al., 2013; Reiners et al., 2004).

In sample TS01 from the eastern coastal intrusion, three out of four grains yielded comparable earliest Late Cretaceous ZHe ages from ~73 ± 4.5 to 97 ± 6.0 Ma. One grain with high-eU yielded an apparent outlier value of 47 ± 2.9 Ma, which is treated as minimum constraints for thermal peaks, possibly owing to the factor/s mentioned above. Even though samples TS01 and YX02 also display a relatively high value of eU (e.g., Dnyanada et al., 2020) and show a narrow dispersion in the ages of their individual grains (73 ± 4.5 to 98 ± 6.0 Ma and 89 ± 5.5 to 98 ± 6.1 Ma, respectively), the corrected age for each sample are consistent with previous ZHe datasets (147 ± 11-75 ± 6 Ma) from northern Guangdong province (Shi et al., 2022; Tao et al., 2017).

However, regardless of different lithology and magmatic/stratigraphic ages, the ZHe single grain ages mainly cluster within the 90–100 Ma range (Figure 6). This records the earliest stage of erosional cooling and represents a phase of

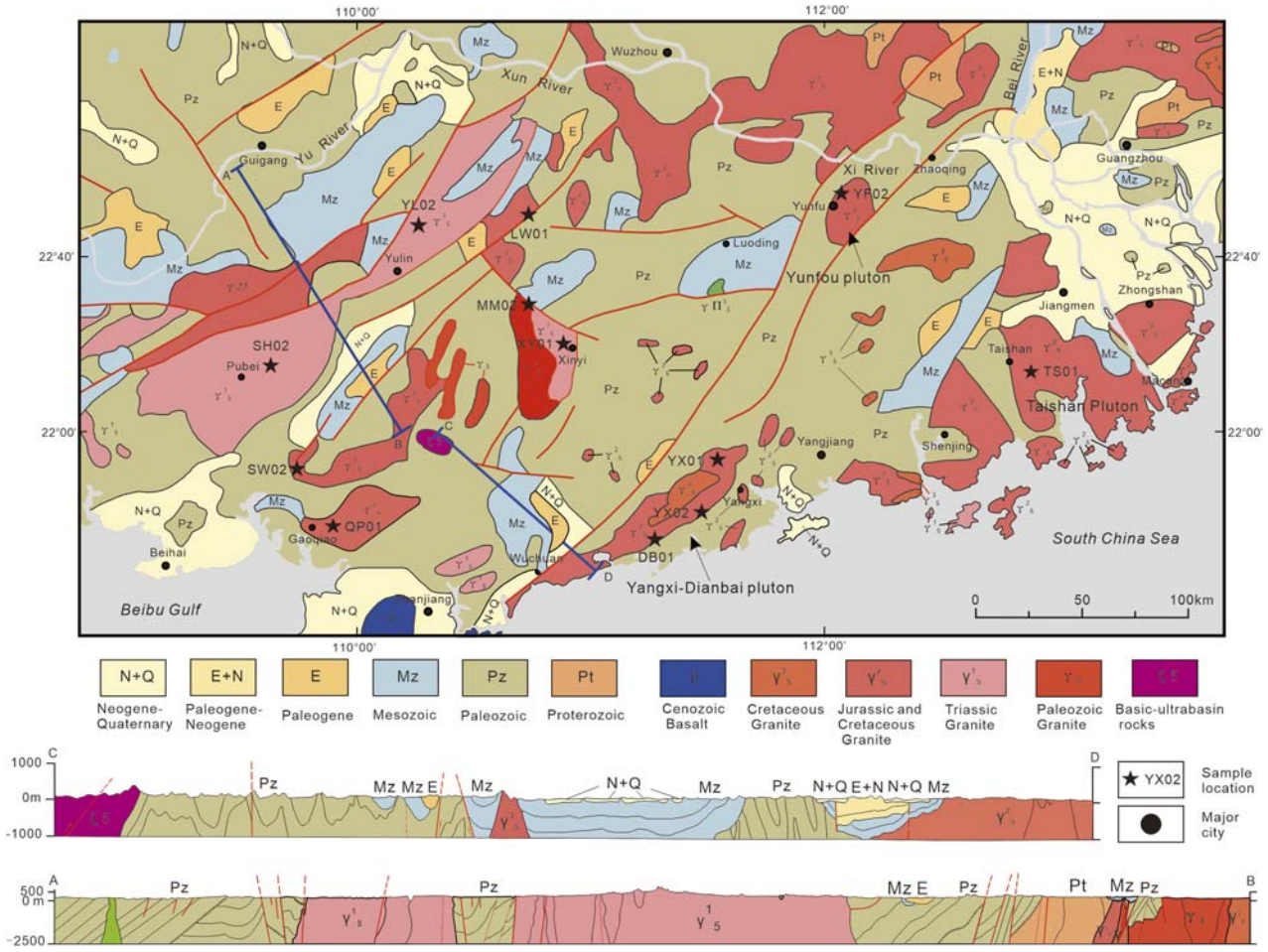

FIGURE 2
Simplified geological map and geological profiles showing regional distributions of rocks in the Cathaysian coastal mountains at sampling locations.

tectonic-thermal activity during the Early to Late Cretaceous, rather than emplacement-related cooling. A possible increasing trend southeastwards until close to the Sihui-Wuchuan fault (SWF) was evident in both the AFT and ZHe ages, although the tendency was neither obvious nor strict if the errors were taken into account (Figure 7), especially in the AFT data. A similar spread was reported by Yan et al. (2009) for the northern margin of the SCS but without apparent age trends. The samples with the oldest AFT and ZHe ages were located both sides of the SWF, which suggested that the fault was probably initially activated by extension and rifting since the Late Cretaceous. Whether the geographical age changes are related to faulting is not very clear owing to gaps in the data (Yan et al., 2009). Therefore, the implication of age differences was not speculated further for the AFT/ZHe data.

5 Thermal history modeling

5.1 Modeling strategy

In order to obtain the tectonic thermal evolution since the Late Cretaceous and evaluate the pattern of AFT and ZHe ages of the sampled rocks, inverse thermal history modeling was performed on the HeFTy software version 1.9.3 (Ketcham, 2005) combined with AFT single grain ages and track lengths, and ZHe data if available. The multi-kinetic annealing model of AFT was applied with the track lengths and D_{par} as the kinetic parameter (Ketcham et al., 2007) in order to obtain much more well-fitting paths. The ZHe data was modeled using the He diffusion model of Reiners et al. (2004). Thermal history was generated incorporating two or three initial constraints: a surface temperature of 20°C ± 2°C at present (Shi et al., 2022; Zhao et al., 2025), and the AFT and ZHe data for the sample. Finally, the modeling strategy in this study was to begin with an open-ended model with minimal constraints and then to gradually impose restrictions based on the successive modeling results (Barnes et al., 2006; Shi et al., 2016). Each model was set to obtain 100 good fit paths with a goodness-of-fit (GOF) >0.5 (Ketcham, 2005), shown as the pink curves in Figure 8. If that failed, inversions then considered 200 acceptable paths (GOF >0.05) (green curves). The black curve represents the best fit path. Figure 8 is a graphic summary of representative thermal histories of modeled samples and the measured versus modelled confined track length distributions.

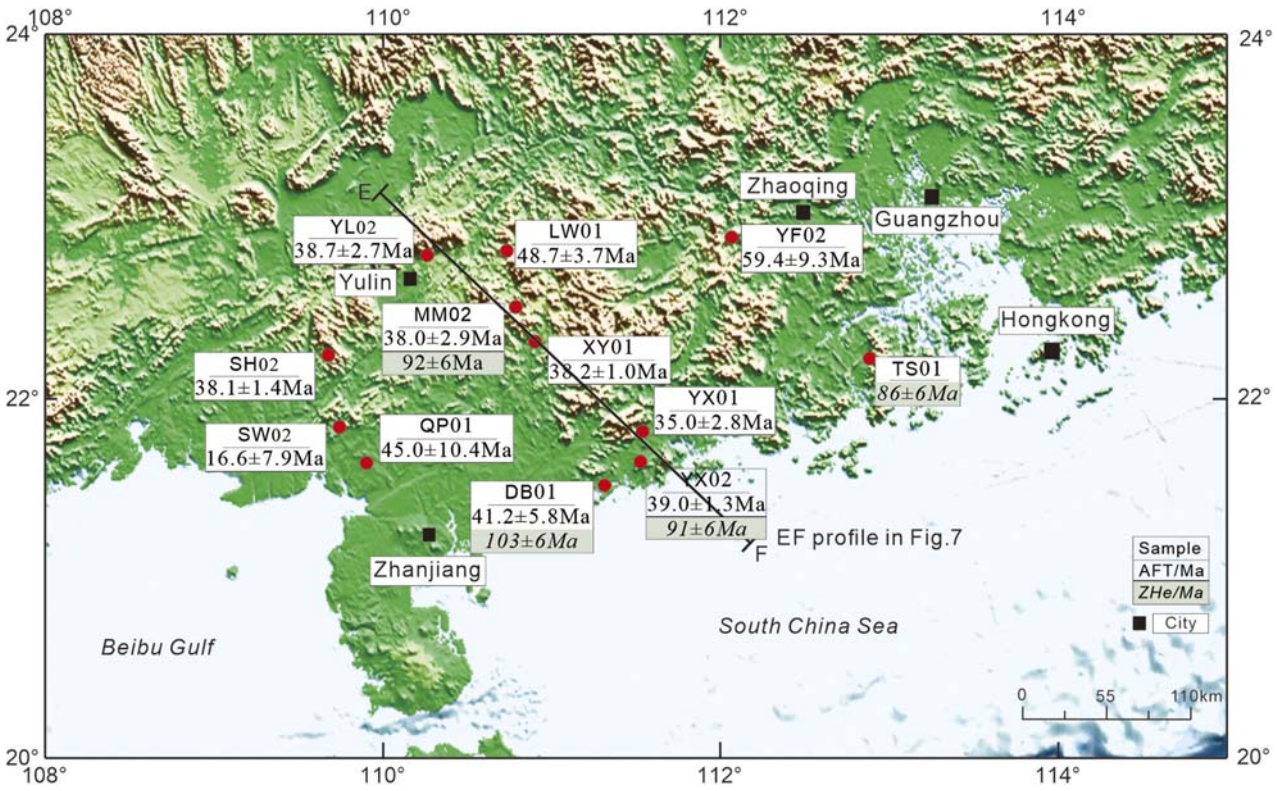

FIGURE 3
Topographic map of southeastern Cathaysian coastal mountains, showing sample locations and AFT pooled/central ages (roman font) and ZHe (italics).

5.2 Modeling results and cooling rate

Modeling results revealed multiple asynchronous cooling stages in the Cathaysian coast mountain since the Late Cretaceous (Figure 8). This implies that most of the samples underwent a generally similar denudation cooling process: (1) widespread Late Cretaceous to Paleocene cooling occurred across the entire coast mountain, whereas the early Yanshanian Yunfu granite sample (YF02) from the northern area shows rapid cooling across the PAZ of ZHe since 100 Ma. This model was based on the AFT data only, because no ZHe age data was available for measurement. (2a) Rapid cooling differed in initial timing at ~60 Ma and ~45 Ma, respectively, (2b) followed by a period of slow cooling with a rough rate of 1°C/Ma from the Oligocene to the middle Miocene. (3) The final stage involved rapid cooling to surface temperature since the middle Miocene, initiated between ~18 and 10 Ma. Similar thermal histories have been reported from many parts of the Cathaysian Block (e.g., Li and Zou, 2017; Shi et al., 2022; Tao et al., 2017; 2019; Yan et al., 2009).

However, the modeling results also suggested that samples XY01 and YX02 showed a prolonged and slow cooling throughout the Cretaceous and Paleogene, followed by a pronounced rapid cooling episode commencing in the Eocene, resulting from erosion of the rock mass, albeit with a timing discrepancy. The samples cooled to surface temperatures during the Oligocene and have maintained thermal stability thereafter. The modeling results demonstrate that exhumation processes along rift shoulders/footwalls exhibited heterogeneous and asynchronous characteristics, whether occurring unilaterally or bilaterally within the rift basin system.

Cooling rates based on good-fit path envelopes display complex spatial and temporal variation. Most of samples experienced relatively high cooling rates (>2.5°C/Ma) during the Paleocene–Eocene and again in the Neogene–Quaternary, with a conspicuously lower rate (<1°C/Ma) during the Oligocene. Exceptions were samples XY01 and YX02, which gave evidence of rapid cooling (>3.8°C/Ma and ~2.3°C/Ma, respectively) in the Oligocene.

6 Discussion

6.1 Timing constraints on extensional structures

It is known that large-scale extension took place in the South China Block because of the rollback of the paleo-Pacific slab and/or other formation mechanisms beginning in the Cretaceous (Figure 9). This is confirmed by the distribution of sedimentary strata and the contact relationships (Wang et al., 2020a), tectonic characteristics (Li et al., 2013), magmatism and geochemistry (Guo et al., 2021; Li et al., 2013). Although the exact onset of extensional deformation owing to the rollback of paleo-Pacific slab under the SE China Plate is generally considered to be no later than

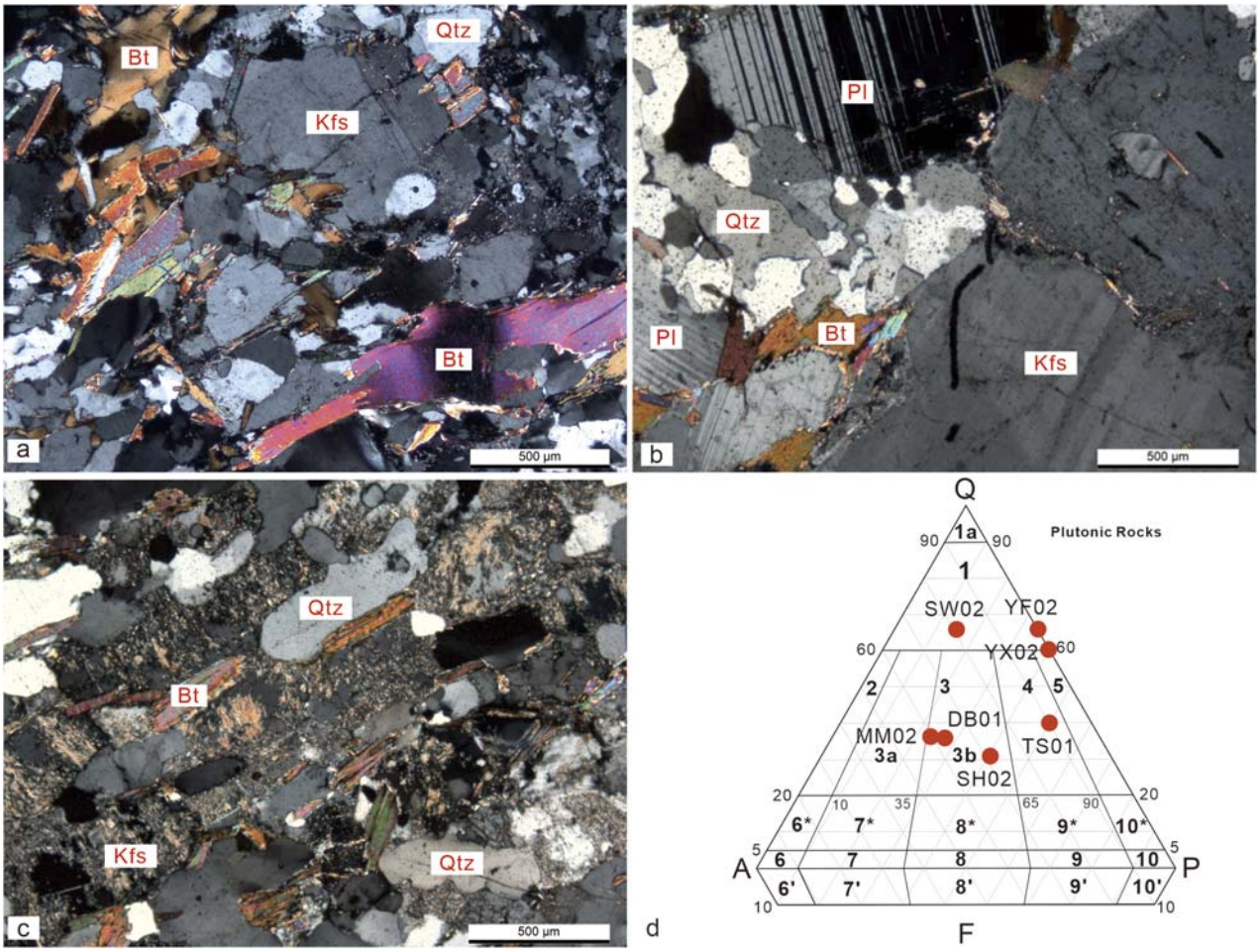

FIGURE 4
Representative micrographs of rocks from: **(a)** Yangxi-Dianbai pluton; **(b)** Yunfou pluton; and **(c)** Taishan pluton. **(d)** the QAPF model diagram of plutonic rocks with locations of some samples. QTZ = quartz; Pl = plagioclase; Kfs = K-feldspar; Bt = biotite.

~110 Ma (Li et al., 2015; Liu et al., 2016), it is still not clear how long the extensional tectonism has lasted (Wang et al., 2020b).

During the Late Cretaceous, large-scale basins produced by synchronous extension (Wang et al., 2020b) were mainly filled with red-colored sandstone, siltstone and mudstone, with evaporative minerals (gypsum and halite, etc.). These extensional basins, such as the Sanshui and Maoming Basins, were generally influenced by the NE to NNE-trending synsedimentary normal faults (Li et al., 2012; Shu et al., 2009), developing distinct regional unconformities between Cretaceous red beds and Eocene sandstones (GBGMR, 1988). Intramontane Cenozoic strata, fluvial and lacustrine sediments were also scattered around the small-scale rift basins (Tao et al., 2019). Paleocene deposition occurs only in a few places, indicating a marked transition in depositional systems between the Late Cretaceous and the Paleogene.

Furthermore, there is a notable inflection point in the thermal history inversion cooling curve at 60 Ma and a significant change in the cooling rate as a consequence. This phase (~75–60 Ma) previously identified by Yan et al. (2009) using the low-temperature thermochronology from the coast to the intracontinental region in the north of the South China Sea. A similar change in cooling rate has also been proposed for the region around the Pearl River Estuary Basin (Li and Zou, 2017), giving the inflection point at ~60 Ma. Tao et al. (2019) found a change in the cooling rate in the Cathaysian Block from slow cooling in the Cretaceous to rapid cooling during the Paleocene-Eocene.

In general, tectonic inversion cannot be distinguished by the change of cooling rate inferred from thermochronological data alone, because either transtension or transpression may contribute to accelerated bedrock exhumation (e.g., Wang et al., 2020b). However, an obvious change in both the cooling rate and the sedimentation indicates a change in the tectonic environment. For example, Shi et al. (2011) and Tao et al. (2019) reported a transition of tectonic setting from extension to rifting between the Cretaceous and the Paleogene.

Therefore we argue that combining low temperature thermochronology with contemporaneous sedimentary records indicated that major Late Cretaceous extension along the coastal mountains in the Cathaysian Block may have continued until ~60 Ma. Of course, more comprehensive studies are still required to decipher the framework of the tectonic evolution of SE China.

TABLE 2 Measurement results of the apatite fission track.

Sample No.	No. of grains	N_s	ρ_s [cm^{-2}]	[1]Pooled ^{238}U [ppm]	D_{par} [μm]	[b]P(χ^b)	[c]Pooled age [Ma ± 1σ]	[d]Central age [Ma ± 1σ]	N_{length}	[e]Mean track length	St.Dev. [μm]
DB01	15	103	1.441E+05	7.49 ± 5.94	1.14	0.58	41.2 ± 5.8	43.9 ± 4.5	89	13.19 ± 0.15	1.38
LW01	40	333	1.985E+05	8.49 ± 3.43	1.14	0.12	48.7 ± 3.7	51.3 ± 3.4	27	11.82 ± 0.5	2.6
MM02	19	553	7.600E+05	43.11 ± 14.33	1.27	0.00	36.2 ± 2.9	38.0 ± 2.9	75	13.13 ± 0.17	1.46
QP01	5	50	4.128E+05	16.91 ± 10	1.19	0.07	45.0 ± 10.4	51.9 ± 7.6	9	12.86 ± 0.28	0.84
SH02	34	1,639	1.614E+06	90.84 ± 29.29	1.28	0.00	37.9 ± 1.6	38.1 ± 1.4	129	12.99 ± 0.14	1.54
SW02	4	19	2.528E+05	34.31 ± 39.31	0.99	0.01	10.6 ± 11.9	16.6 ± 7.9	0	-	-
XY01	46	2,663	1.109E+06	63.30 ± 14.48	1.33	0.01	37.9 ± 1.0	38.2 ± 1.0	141	13.7 ± 0.1	1.54
YF02	19	151	2.242E+05	7.4 ± 4.92	1.19	0.09	59.4 ± 9.3	63.5 ± 6.7	92	12.9 ± 0.2	1.86
YL02	7	72	6.013E+05	32.96 ± 3.16	1.20	0.93	38.7 ± 2.7	39.2 ± 4.7	17	13.4 ± 0.3	1.35
YX01	19	210	4.630E+05	26.60 ± 27.87	1.11	0.50	35.0 ± 2.8	36.3 ± 2.7	26	12.5 ± 0.4	2.07
YX02	40	2,188	1.357E+06	77.77 ± 45.15	1.39	0.00	37.9 ± 1.3	39.0 ± 1.3	102	13.1 ± 0.2	1.69

[a]Pooled U is the uranium concentration measured by LA-ICP-MS.
[b]P (χ2) is probability obtaining chi-square value for n degrees of freedom (Galbraith, 1981).
[c]Pooled age estimated after Hasebe et al. (2004).
[d]Central age calculated with RadialPlotter v. 9.5 (Vermeesch, 2009).
[e]Mean confined track length (Ketcham et al., 2007) after Cf irradiation.

10.3389/feart.2025.1597461

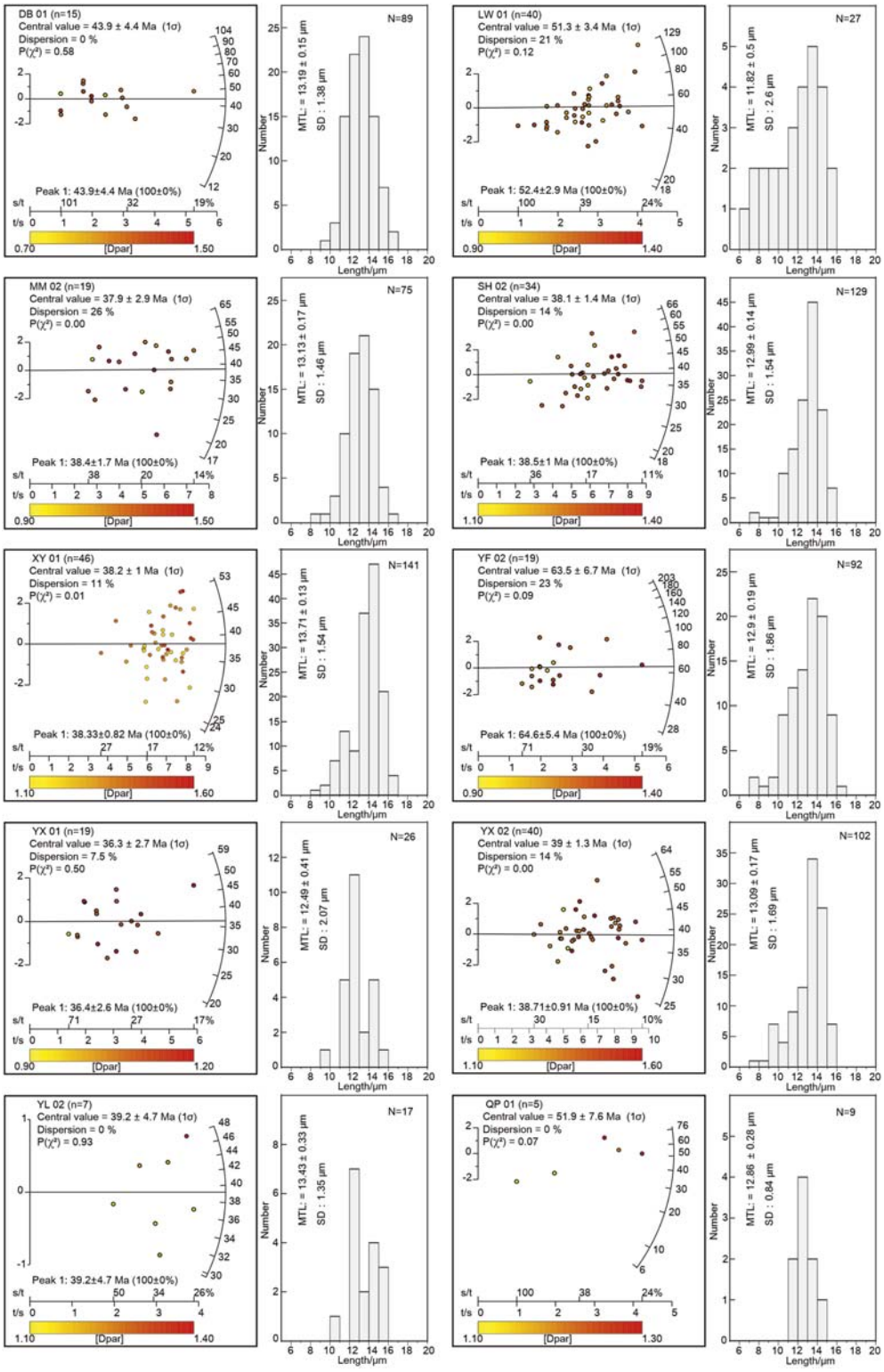

FIGURE 5
Radial plots of AFT age of single grains with D_{par} (right-hand curve), with relative error (%) shown as distance from the curve; and histograms of confined fission track lengths.

For the continental interior, Wang et al. (2020b) argued that extension may have finally ceased around 100 Ma, as evidenced by the dome structure and $^{40}Ar/^{39}Ar$ ages of biotite and muscovite and AFT and ZFT age. Similar results were found in Hengshan (Li et al., 2013) and the Lushan dome (Lin et al., 2000), all interpreted to be related with the asynchronous rollback of the paleo-Pacific

TABLE 3 Zircon (U-Th)/He results from the Cathaysian coastal mountains.

Sample	^{4}He (ncc)	Mass (mg)	[a]F_T	U Ppm	Th ppm	Th/U ratio	[b][eU] ppm	Corrected age (Ma)	Error (±1σ)	Grain length/ L (μm)	Grain half width/ W (μm)	[c]Crystal Radius (μm)	[d]Crystal Morphology
TS01	43.560	0.0046	0.74	706.9	378.0	0.53	795.7	96.9	6.0	226.9	38.0	48.8	2T
TS01	100.123	0.0058	0.78	1811.8	573.1	0.32	1946.5	72.6	4.5	210.4	46.8	57.4	2T
TS01[e]	135.616	0.0038	0.75	5,484.6	3,139.1	0.57	6,222.3	47.4	2.9	175.3	42.2	51	2T
TS01	106.277	0.0041	0.74	1879.8	1,116.4	0.59	2,142.2	97.6	6.0	197.1	40.1	50	2T
weighted mean age: 85.7 ± 6.2 Ma													
YX02	35.127	0.0087	0.80	347.0	195.1	0.56	392.8	84.0	5.2	232.4	55.5	67.2	2T
YX02	207.977	0.0121	0.82	1,571.0	35.0	0.02	1,579.2	88.8	5.5	294.5	55.1	69.6	2T
YX02	314.867	0.0101	0.82	2,578.6	37.9	0.01	2,587.6	98.2	6.1	260.9	54.7	67.9	2T
YX02	273.428	0.0098	0.80	2,385.2	29.2	0.01	2,392.0	95.3	5.9	305.4	47.1	61.2	2T
weighted mean age: 90.9 ± 5.6 Ma													
DB01	30.719	0.0092	0.81	276.0	55.2	0.20	289.0	94.3	5.8	255.9	52.5	65.3	2T
DB01	44.819	0.0099	0.81	340.3	32.2	0.09	347.8	106.2	6.6	271.6	52.1	65.6	2T
DB01	45.160	0.0136	0.82	252.6	44.5	0.18	263.1	103.0	6.4	319.1	55.3	70.7	2T
DB01	76.722	0.0101	0.79	520.5	105.8	0.20	545.4	113.3	7.0	322.8	46.1	60.5	2T
weighted mean age: 103.3 ± 6.4 Ma													
MM02	25.687	0.0083	0.81	266.4	87.3	0.33	286.9	88.4	5.5	231.8	53.8	65.5	2T
MM02	53.417	0.0056	0.77	726.0	176.0	0.24	767.4	101.3	6.3	227.8	42.6	53.8	2T
MM02	36.962	0.0043	0.75	770.2	61.3	0.08	784.6	90.1	5.6	207.8	39.0	49.2	2T
MM02	38.827	0.0062	0.77	556.1	54.5	0.10	568.9	89.1	5.5	246.2	42.7	54.6	2T
weighted mean age: 91.7 ± 5.7 Ma													
Fish Canyon Tuff reference material													
FCT	5.816	0.0042	0.76	336.6	196.0	0.58	382.6	29.5	1.8	175.3	45.7		2T
FCT	3.810	0.0019	0.64	474.1	264.9	0.56	536.3	30.7	1.9	147.9	31.7		2T

[a]F_T, is an ejection of alpha particle correction factor (after Farley et al., 1996).
[b]The eU is the effective uranium concentration determined by [U ppm + 0.235 Th ppm].
[c]The crystal radius is spherical equivalent radius = (3*W*L)/2*(W + L) from Beucher et al. (2013).
[d]Crystal morphology - 2T, 2 terminations.
[e]Data not included in calculation of weighted mean age by Isoplot v. 4.0 (Ludwig, 1991).

Plate. In addition, the discovery that late Mesozoic magmatic rocks are younger toward the SE offshore has also been attributed to southeastward migration of magmatic activity in response to slab rollback (Wang et al., 2020b; Zhou et al., 2006). This thermal-tectonic scenario is also supported by the eastward migration of the Yanshanian (Jurassic-Cretaceous) subduction along the continental margin of the Cathaysian block as determined by analysis of gravity and magnetic anomalies (Lu et al., 2022).

6.2 Geodynamic mechanisms of Late Cretaceous tectonism

The modeling results suggested significant regional cooling during ~100–60 Ma (phase 1, Figure 9) with spatial heterogeneity controlled by localized tectonic regimes and associated magmatic activity. Sample YF02 collected from the early Yanshanian Yunfu gneissic pluton revealed a different cooling process, which was

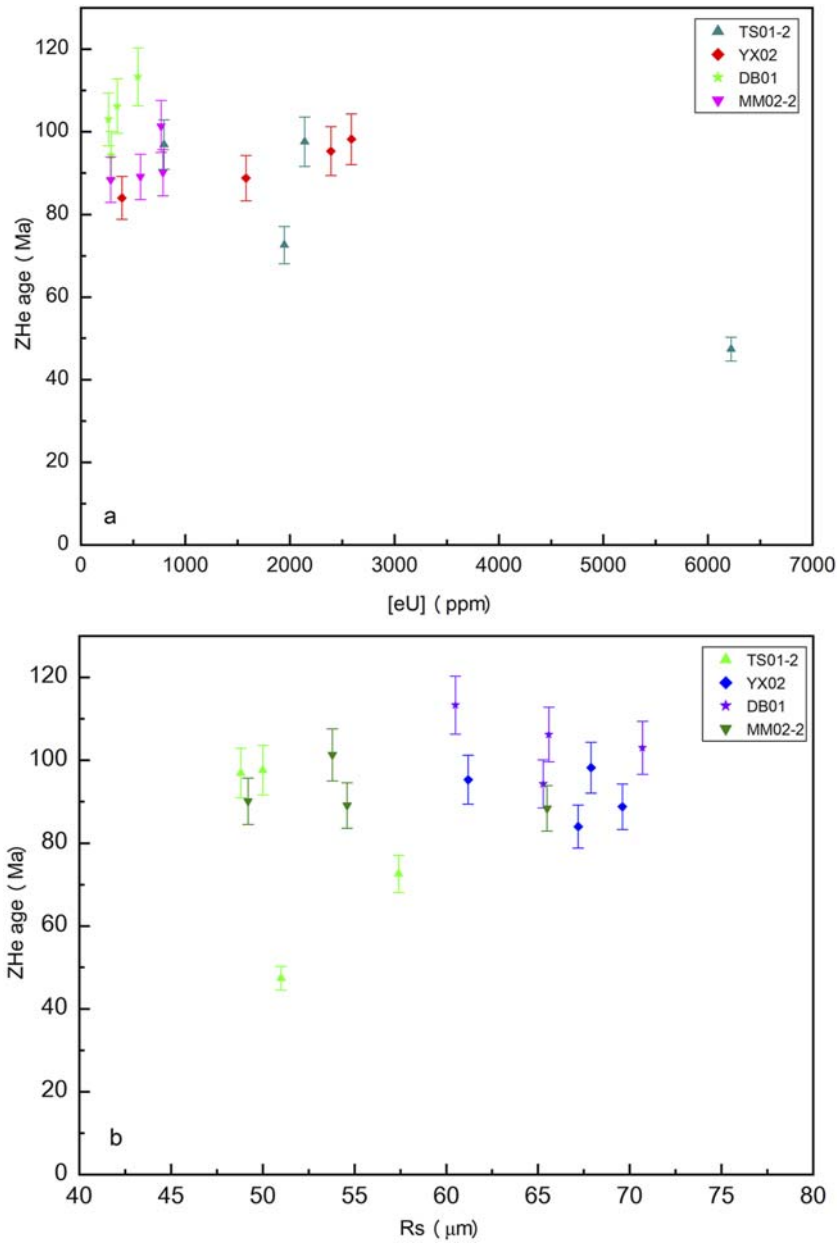

FIGURE 6
(A) ZHe single grain age vs eU. The lack of obvious correlation suggests little effect on grain ages from radiation damage; **(B)** ZHe grain age vs crystal radius.

attributed to local extension and the activity of NE/NNE-trending fault systems located to the east and west of Wuchuan-Sihui fault. However, AFT and ZHe data reported by Yan et al. (2009) indicated a relatively slow cooling event in the Late Cretaceous (~100–75 Ma for intracontinental areas versus ~60 Ma for coastal domains) at the northern margin of the SCS. A little further to the northwest, Tao et al. (2017); Tao et al. (2019) concluded that slow cooling occurred in the Cretaceous, followed by rapid cooling in the Paleocene, and considered the slow cooling rate is resulted from the rebound of the central Cathaysian block leading to lithospheric extension. Apatite and zircon fission track thermochronology of the southeastern margin of coastal mountains also suggest a slow cooling history during 94–60 Ma (Li and Zou, 2017). The relatively slow cooling phase may be generally related to the numerous Cretaceous extensional basins in the Cathaysian Block (Li et al., 2014). Furthermore, the NE to NNE-trending normal faults, dome structures, and A-type granite magmatism in the Cathaysian Block suggest that the Indosinian orogenic belts experienced significant extension during the Cretaceous (Guo et al., 2021; Wang et al., 2020b).

Rollback of the subducted Paleo-Pacific Plate has been widely invoked to explain late Cretaceous–Paleogene extension and magmatism in the South China Block, as evidenced by seaward-younging granite ages and syn-magmatic normal faulting (Guo et al.,

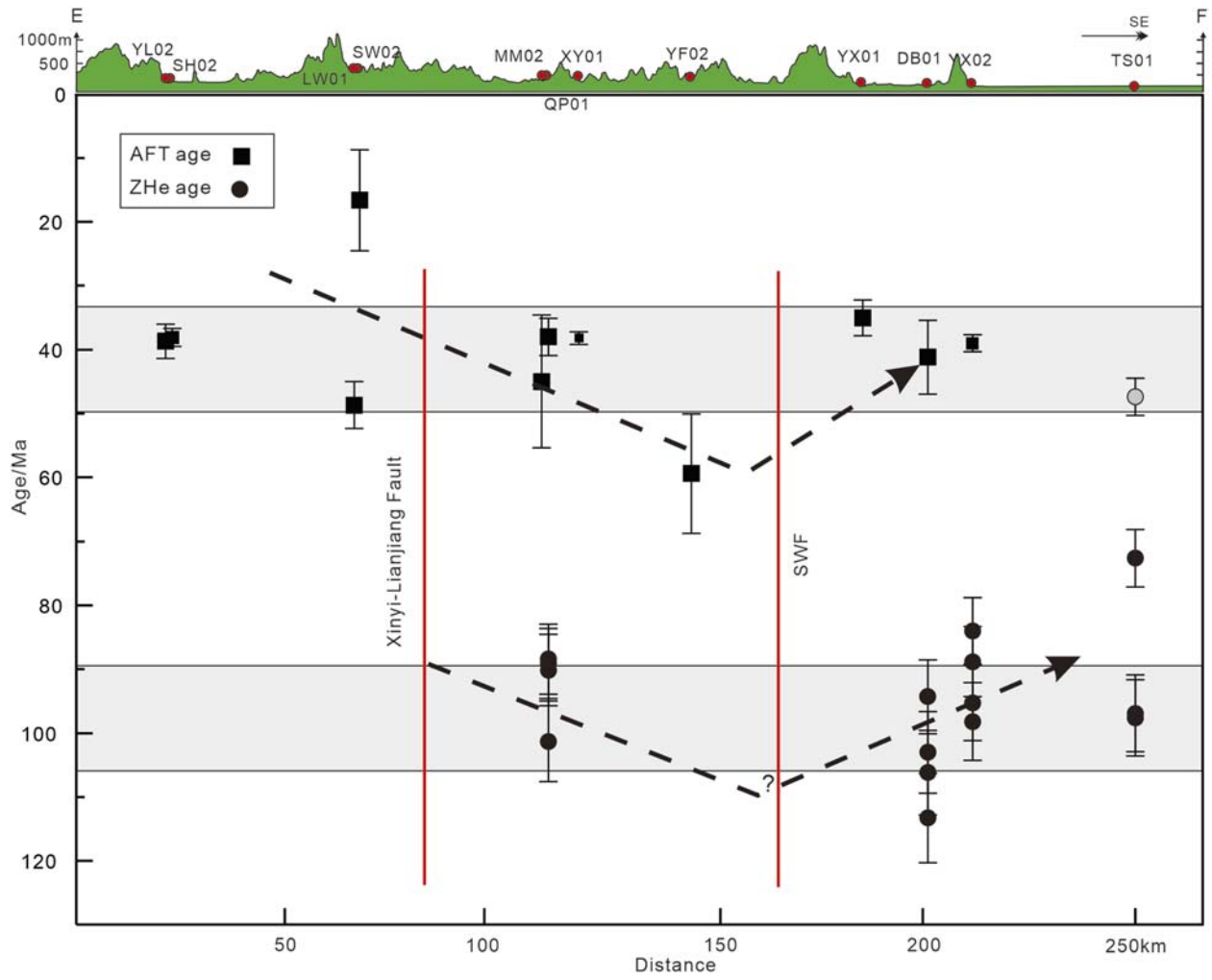

FIGURE 7
Spatial pattern of AFT and ZHe ages. Location of inflexion is uncertain due to data gap. (The gray circle represents the outlier result for sample TS01 and is not caused by high eU).

2021; Li et al., 2015; Liu et al., 2016; Zeng et al., 2016), although other dynamic models have been proposed (e.g., Liu et al., 2013; Wang et al., 2020b). Furthermore, the diachronous extension, delayed by ~40 Ma before arriving at the inflection point in the distal Cathaysian block likely terminated at ~60 Ma in the SE coastal orogenic belt, as discussed above (Wang et al., 2020b).

6.3 Paleocene-Eocene cooling and Oligocene thermal stasis

The AFT ages of granitic samples vary from 36.3 ± 2.7 to 63.5 ± 6.7 Ma (mean track length 12.99 ± 1.54 to 13.7 ± 1.54 μm), and apatite (U-Th)/He (AHe) ages are mostly between 30 and 40 Ma from inland near Nanxiong to the coast east of Hong Kong (Yan et al., 2009), which suggest a rapid cooling in the early Paleogene. An accelerated exhumation across the coastal region of South China probably commenced in the Paleogene (phase 2A). Modeling results in this study also reveal that most samples experienced rapid cooling since the Paleogene or in the early Eocene. Samples of sandstone and granite from the northern Guangdong region indicated a stage of rapid cooling during the Paleocene and Eocene (Tao et al., 2017; Tao et al., 2019). Briefly, rapid cooling occurred from the latest Cretaceous through the Eocene period is suggested by the thermochronology across the central Cathaysian Block (Yan et al., 2009).

At around 60 Ma, the Pacific Plate initiated its replacement of the subducting paleo-Pacific Plate beneath the Eurasian Plate, accompanied by eastward retreat of the subduction system. Concurrently, the Indo-Eurasian collision induced eastward uplift in the northeastern Tibetan Plateau, generating sinistral (left-lateral) shear deformation. These combined tectonic processes ultimately led to intense rifting throughout South China. (Figure 9) (Li et al., 2013; Suo et al., 2019; Wang et al., 2020a). It has been reasonably suggested that the Paleocene-to-Eocene rapid cooling event was accompanied by episodic continental rifting (Shi et al., 2011; Tao et al., 2019; Zhou et al., 1995) initiating at the coast and propagating southeastward, as evidenced by Eocene

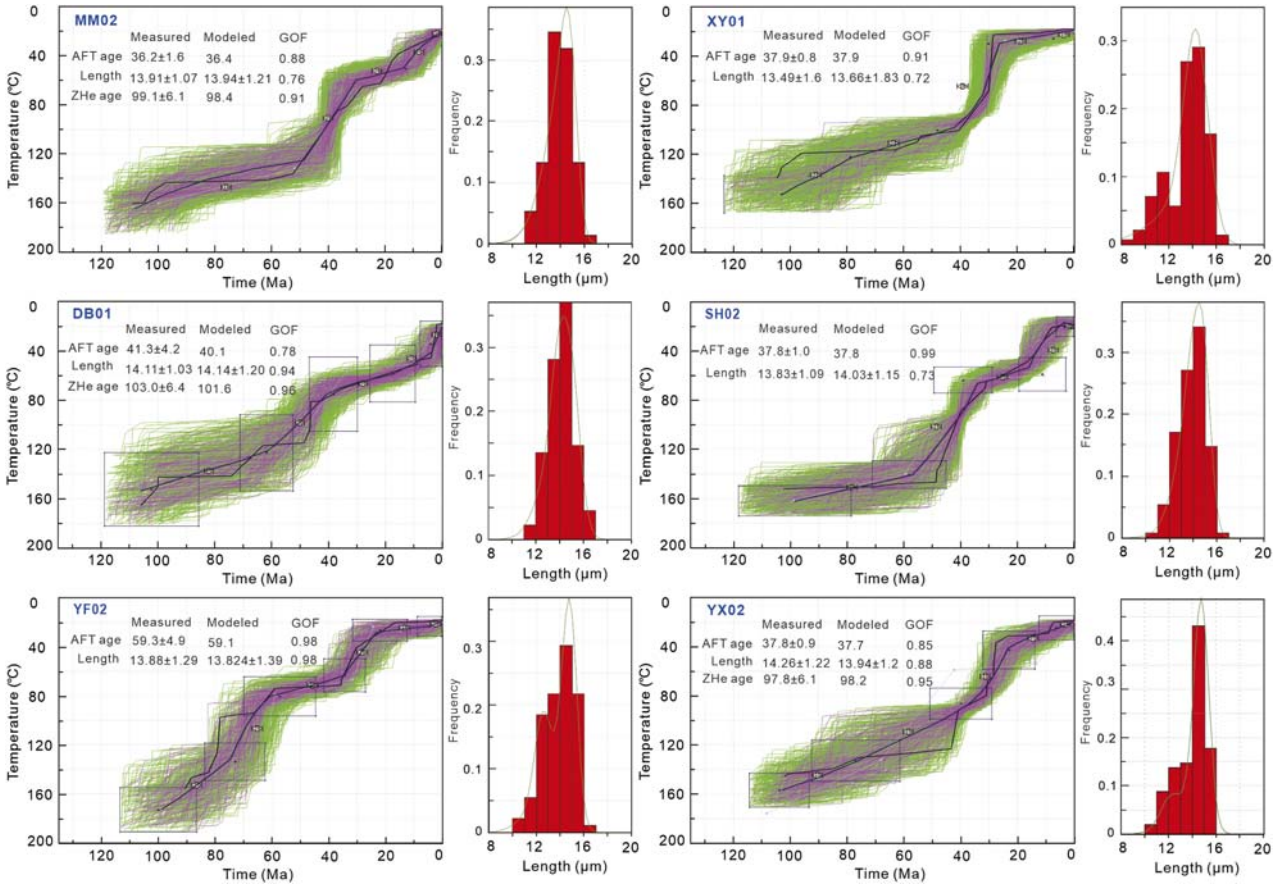

FIGURE 8
Graphic summaries of thermal history modeling results and sample track lengths. (Pink lines = good fit paths; green lines = acceptable fit; black line = best fit; GOF = goodness-of-fit) (Ketcham, 2005).

volcanism found in the NE-striking Sanshui Basin. Therefore, rapid exhumation occurred along rift footwall/shoulders on one or both sides of the rift basins during that time, while the adjacent rift basins (e.g., the Sanshui Basin) were subjected to rift-related volcanism and subsidence. This rift event has previously been considered as a precursor to the opening of the SCS in the mid-Cenozoic (Li et al., 2012; Tao et al., 2019). However, rapid exhumation along rift footwall/shoulders may be attributed to normal faulting, given the fault-controlled nature of rifting. The magnitude of fault-related denudation exhibits a negative correlation with distance from the fault. Cooling rates based on the modeling t-T path envelopes have demonstrated a complex spatial variation pattern during Paleogene and Eocene as well.

Thermal history modeling results showed that most samples experienced spatially differential cooling due to the continental rifting during the Paleocene and Eocene, followed by a slow cooling stage in the mid-Cenozoic (phase 2B, Figure 9). Temporally this phase of negligible erosion basically coincided with a major phase of extension (~40–15 Ma) in the SCS Basin initiated in the Late Eocene, which caused rapid subsidence along the northern basin margins of the SCS (e.g., Yan et al., 2009), and opening of the SCS ca. 37–17 Ma. Nd isotope studies at ODP [184] Site 1,148 indicated that the erosional sources were predominantly derived from distal continental interiors (e.g., Yangtze block) rather than proximal coastal mountains during that time period (Clift et al., 2002; Li et al., 2003). Meanwhile, Chen et al. (2022) also concluded that the provenance of northern South China Sea marginal basins had migrated from the Cathaysian coastal mountains to the inland of the South China Block since the Eocene by means of detrital zircon U-Pb ages analysis. However, samples YF02, XY01 and YX02 record a transient thermal history of rapid cooling to surface temperature coincident with continuous rifting (phase 2A), although the rift center had migrated to the sea basin of the SCS. Assuming identical geothermal gradients, phase 2B exhibits significantly lower denudation magnitudes compared to phase 2A, implying progressive migration of erosional provenance.

6.4 Late Cenozoic rock uplift and climatic transition

Thermal modeling results indicated that most samples underwent a relatively rapid cooling event again during the Late Cenozoic (Figure 8). An accelerated regional exhumation was probably initiated in the middle Miocene (phase 3). The Miocene tectono-thermal cooling event has been reported for a broad region

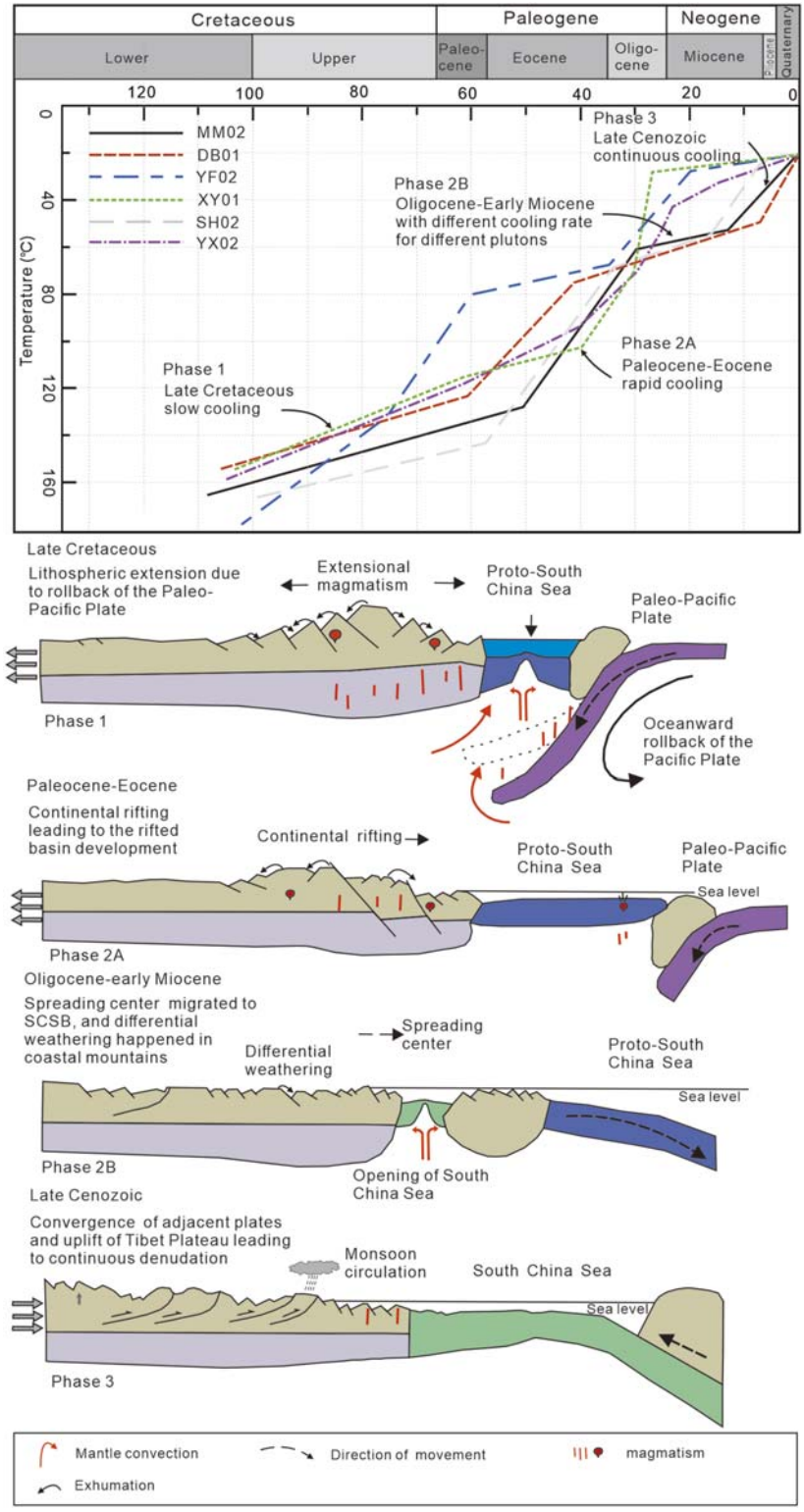

FIGURE 9
Schematic diagram showing the thermal histories incorporating the time-temperature trajectories in Figure 8, and the tectonic and geomorphic evolution of SE China coastal mountains since the late Cretaceous. The tectonic cartoons are modified from Tao et al. (2017); Shi et al. (2022).

from the Yangtze Plate to the Cathaysian southeastern coastal region (e.g., Shi et al., 2011; Yan et al., 2009), although the exhumation magnitude was much less than in the Late Cretaceous-Paleogene. It has been interpreted as the far-field effect of the collision between the India-Eurasia Plates (Shi et al., 2016; Tao et al., 2019; Yan et al., 2009).

However, it has been suggested that the Cretaceous and Paleogene semi-desert sediments of red beds with evaporites (Shu et al., 2009; Wang et al., 2020b; Zhou et al., 2006) were absent in the Neogene strata in south China due to the strengthening of the monsoon climate in East Asia, which commenced around 23 Ma (e.g., Clift et al., 2008a; 2008b). Around the same time, the SCS margin basins displayed a remarkable increase in sediment accumulation rate consistent with increasing regional denudation, occurring simultaneously with tectonic inversion in the Pearl River Mouth Basin (Zhou et al., 1995). From this it is inferred that there was a clear shift of climate in south China from semi-arid environment to monsoonal, and a more erosive climate due to the topographic uplift of the Tibetan Plateau (Figure 9), which also resulted in the absence of red beds with evaporites. Additionally, the tectonic explanation is related to the far-field effects of the Indian-Asian continental convergence and the collision between the Philippine island arc and Eurasian Plate beginning in the late Miocene to Pliocene (Sibuet et al., 2002; Yan et al., 2009) and is referred to as the 'multiple-plates interaction' (Wang et al., 2020a). However, this period of cooling occurred completely beyond the partial annealing zone of the AFT.

7 Conclusion

The proposed new low temperature thermochronological ZHe and AFT data provided novel insights into the tectono-thermal evolution of the Cathaysian coastal mountains on the continental margin of the South China Sea. ZHe dating revealed ages of 90–100 Ma for Mesozoic granitic rocks, interpreted as reflecting the rollback of the subducted paleo-Pacific Plate. AFT ages of granitic samples varied from 36.3 ± 2.7 to 63.5 ± 6.7 Ma, with mean track lengths 12.99 ± 1.54 to 13.7 ± 1.54 μm. These suggested that a period of rapid cooling took place during the Paleocene and Eocene.

AFT and ZHe ages and thermal history modeling revealed a multi-stage and asynchronous cooling process. Most samples from the coastal mountains in the Cathaysian Block experienced complex cooling episodes: at first relatively slow cooling, then rapid cooling, followed by a second period of slow cooling, then final regional accelerated cooling since the Late Cretaceous. The relatively slow cooling was related to Mesozoic extension, consistent with lithospheric rebound after the rollback of the subducted paleo-Pacific slab. This exhumation was determined by faults (e.g., Sihui-Wuchuan fault). The extension may have finally ceased at ~60 Ma, as inferred from the transition of the paleo-geographical environment and the inflexion point in the cooling envelope. The rapid cooling in the Paleocene-Eocene was also temporally interpreted as being coincident with continental rifting in the southeastern region of south China, and has been considered to be a precursor to the opening of the South China Sea. As the episodic continental rifting migrated southward, the cooling rate decreased gradually. Finally, a regional accelerated exhumation was initiated in the late Cenozoic by the far-field effect of the Indian–Asian continental convergence and the collision between the Philippine island arc and the Eurasian Plate.

Data availability statement

The original contributions presented in the study are included in the article/supplementary material, further inquiries can be directed to the corresponding authors.

Ethics statement

The manuscript presents research on animals that do not require ethical approval for their study.

Author contributions

HS: Formal Analysis, Project administration, Data curation, Writing – original draft, Methodology, Visualization, Investigation, Funding acquisition, Writing – review and editing, Conceptualization, Supervision. HX: Investigation, Writing – review and editing, Data curation, Supervision, Funding acquisition, Resources, Formal Analysis, Validation. WZ: Data curation, Writing – review and editing, Investigation, Visualization, Supervision, Resources. TL: Project administration, Resources, Validation, Writing – review and editing, Supervision, Funding acquisition. DK: Funding acquisition, Formal Analysis, Project administration, Supervision, Writing – review and editing, Data curation. CB: Investigation, Visualization, Formal Analysis, Validation, Writing – review and editing. LL: Data curation, Visualization, Software, Writing – review and editing, Formal Analysis.

Funding

The author(s) declare that financial support was received for the research and/or publication of this article. This work was supported by the National Natural Science Foundation of China (grants Nos. 41776024, 41766001, 41962019); the Program for Scientific Research Start-up Funds of Guangdong Ocean University (grant No. E15171) and Marine Science Research Team Project of Guangdong Ocean University (grant No. 002026002004); the Guangdong Provincial College Innovation Team Project (grant No. 2019KCXTF021) and the First-class Discipline Plan of Guangdong Province (grant No. 080503032101 2, 31420003); Key Laboratory of Marine Mineral Resources, Ministry of Natural Resources, Guangzhou (grant No. KLMMR-2024-K02) and Natural Science Basic Research Program of Shaanxi (grant No. 2024JC-YBQN-0684).

Acknowledgments

The authors would like to express sincere gratitude to the editor and reviewers for their insightful suggestions and constructive

feedback, which have significantly contributed to the improvement and refinement of this manuscript and to Professor Barry Kohn and his team for conducting the apatite fission track and zircon (U-Th)/He age analyses.

Conflict of interest

The authors declare that the research was conducted in the absence of any commercial or financial relationships that could be construed as a potential conflict of interest.

Generative AI statement

The author(s) declare that no Generative AI was used in the creation of this manuscript.

Publisher's note

All claims expressed in this article are solely those of the authors and do not necessarily represent those of their affiliated organizations, or those of the publisher, the editors and the reviewers. Any product that may be evaluated in this article, or claim that may be made by its manufacturer, is not guaranteed or endorsed by the publisher.

References

Anderson, A., Hodges, K. V., and Soest, M. C. (2017). Empirical constraints on the effects of radiation damage on helium diffusion in zircon. *Geochimica Cosmochimica Acta* 218, 308–322. doi:10.1016/j.gca.2017.09.006

Barckhausen, U., Engels, M., Franke, D., Ladage, S., and Pubellier, M. (2014). Evolution of the South China Sea: revised ages for breakup and seafloor spreading. *Mar. Petroleum Geol.* 58, 599–611. doi:10.1016/j.marpetgeo.2014.02.022

Barnes, J. B., Ehlers, T. A., McQuarrie, N., O'Sullivan, P. B., and Pelletier, J. D. (2006). Eocene to recent variations in erosion across the central andean fold-thrust belt, northern Bolivia: implications for plateau evolution. *Earth Planet. Sci. Lett.* 248, 118–133. doi:10.1016/j.epsl.2006.05.018

Beucher, R., Brown, R. W., Roper, S., Stuart, F., and Persano, C. (2013). Natural age dispersion arising from the analysis of broken crystals: part II. Practical application to apatite (U–Th)/He thermochronometry. *Geochimica Cosmochinica Acta* 120, 395–416. doi:10.1016/j.gca.2013.05.042

Chen, Y., Meng, J., Liu, H., Wang, C. S., Tang, M., Liu, T., et al. (2022). Detrital zircons record the evolution of the Cathaysian coastal Mountains along the south China margin. *Basin Res.* 34 (2), 688–701. doi:10.1111/bre.12636

Clift, P., Lee, J. I., Clark, M. K., and Blusztajn, J. (2002). Erosional response of South China to arc rifting and monsoonal strengthening: a record from the South China Sea. *Mar. Geol.* 184, 207–226. doi:10.1016/s0025-3227(01)00301-2

Clift, P. D., Hodges, K. V., Heslop, D., Hannigan, R., Long, H. V., and Calves, G. (2008a). Correlation of himalayan exhumation rates and Asian monsoon intensity. *Nat. Geosci.* 1, 875–880. doi:10.1038/ngeo351

Clift, P. D., Lee, G. H., Anh Duc, N., Barckhausen, U., Van Long, H., and Zhen, S. (2008b). Seismic reflection evidence for a dangerous grounds miniplate: no extrusion origin for the South China Sea. *Tectonics* 27, TC3008. doi:10.1029/2007tc002216

Dnyanada, S., George, M., Barry, K., Kanchan, P., and Birak, B. (2020). Thermochronological insights into the thermotectonic evolution of Mishmi hills across the dibang valley, NE Himalayan syntaxis. *J. Asian Earth Sci.* 190, 104158. doi:10.1016/j.jseaes.2019.104158

Farley, K., Wolf, R. A., and Silver, L. T. (1996). The effects of long alpha-stopping distances on (U–Th)/He dates. *Geochimica Cosmochimica Acta*, 60, 4223–4230. doi:10.1016/S0016-7037(96)00193-7

Galbraith, R. F. (1981). On statistical models for fission track counts. *Math. Geol.* 13, 471–478. doi:10.1007/bf01034498

GBGMR (Guangdong Bureau of Geology and Mineral Resources) (1988). *Regional geology of the Guangdong province*. Beijing: Geological Press. (in Chinese).

Gleadow, A., Harrison, M., Kohn, B., Lugo-Zazueta, R., and Phillips, D. (2015). The fish canyon tuff: a new look at an old low-temperature thermochronology standard. *Earth Planet. Sci. Lett.* 424, 95–108. doi:10.1016/j.epsl.2015.05.003

Gleadow, A. J. W., and Duddy, I. R. (1981). A natural long term track annealing experiment for apatite. *Nucl. Tracks Radiat. Meas.* 5, 169–174. doi:10.1016/0191-278x(81)90039-1

Guenthner, W. R., Reiners, P. W., Ketcham, R. A., Nasdala, L., and Giester, G. (2013). Helium diffusion in natural zircon: radiation damage, anisotropy, and the interpretation of zircon (U-Th)/He thermochronology. *Am. J. Sci.* 313 (3), 145–198. doi:10.2475/03.2013.01

Guo, F., Wu, Y. M., Zhang, B., Zhang, X., Zhao, L., and Liao, J. (2021). Magmatic responses to Cretaceous subduction and tearing of the paleo-Pacific plate in SE China: an overview. *Earth-Science Rev.* 212, 103448. doi:10.1016/j.earscirev.2020.103448

Hall, R. (2012). Late Jurassic–Cenozoic reconstructions of the Indonesian region and the Indian Ocean. *Tectonophysics* 570, 1–41. doi:10.1016/j.tecto.2012.04.021

Hasebe, N., Barbarand, J., Jarvis, K., Carter, A., and Hurford, A. J. (2004). Apatite fission-track chronometry using laser ablation ICP-MS. *Chem. Geol.* 207 (3-4), 135–145. doi:10.1016/j.chemgeo.2004.01.007

Ketcham, R. A. (2005). Forward and inverse modeling of low-temperature thermochronometry data. *Rev. Mineralogy Geochem.* 58, 275–314. doi:10.2138/rmg.2005.58.11

Ketcham, R. A., Carter, A., Donlick, R. A., Barbarand, J., and Hurford, A. J. (2007). Improved modeling of fission-track annealing in apatite. *Am. Mineralogist* 92, 799–810. doi:10.2138/am.2007.2281

Li, C. S., Arndt, N. T., Tang, Q. Y., and Ripley, E. M. (2015). Trace element indiscrimination diagrams. *Lithosphere* 232, 76–83. doi:10.1016/j.lithos.2015.06.022

Li, J. H., Dong, S. W., Zhang, Y. Q., Zhao, G. C., Johnston, S. T., Cui, J. J., et al. (2016). New insights into Phanerozoic tectonics of south China: part 1, polyphase deformation in the jiuling and lianyunshan domains of the central jiangnan orogen. *J. Geophys. Res. (Solid Earth)* 121 (4), 3048–3080. doi:10.1002/2015jb012778

Li, J. H., Zhang, Y. Q., Dong, S. W., and Johnston, S. T. (2014). Cretaceous tectonic evolution of South China: a preliminary synthesis. *Earth-Science Rev.* 134, 98–136. doi:10.1016/j.earscirev.2014.03.008

Li, J. H., Zhang, Y. Q., Dong, S. W., Su, J. B., Cui, J. J., Shi, W., et al. (2013). The hengshan low-angle normal fault zone: structural and geochronological constraints on the late Mesozoic crustal extension in south China. *Tectonophysics* 606, 97–115. doi:10.1016/j.tecto.2013.05.013

Li, S. Z., Suo, Y. H., Li, X. Y., Zhou, J., Santosh, M., Wang, P. C., et al. (2019). Mesozoic tectono-magmatic response in the East Asian ocean-continent connection zone to subduction of the Paleo-Pacific plate. *Earth-Science Rev.* 192, 91–137. doi:10.1016/j.earscirev.2019.03.003

Li, X. H., Wei, G. J., Shao, L., Liu, Y., Liang, X. R., Jian, Z. M., et al. (2003). Geochemical and Nd isotopic variations in sediments of the South China Sea: a response to Cenozoic tectonism in SE Asia. *Earth Planet. Sci. Lett.* 211, 207–220. doi:10.1016/s0012-821x(03)00229-2

Li, X. M., Wang, Y. J., Tan, K. X., and Peng, T. P. (2005). Meso-cenozoic uplifting and exhumation on yunkaidashan: evidence from fission track thermo-chronology. *Chin. Sci. Bull.* 50, 903–909. doi:10.1007/bf02897385

Li, X. M., and Zou, H. P. (2017). Late Cretaceous-Cenozoic exhumation of the southeastern margin of Coastal Mountains, SE China, revealed by fission-track thermochronology: implications for the topographic evolution. *Solid Earth Sci.* 2, 79–88. doi:10.1016/j.sesci.2017.02.001

Li, Z. X., and Li, X. H. (2007). Formation of the 1300-km-wide intracontinental orogen and post-orogenic magmatic province in Mesozoic South China: a flat-slab subduction model. *Geology* 35, 179–182. doi:10.1130/g23193a.1

Li, Z. X., Li, X. H., Chung, S. L., Lo, C. H., Xu, X., and Li, W. X. (2012). Magmatic switch-on and switch-off along the South China continental margin since the Permian: transition from an andean-type to a Western Pacific-type plate boundary. *Tectonophysics* 532, 271–290. doi:10.1016/j.tecto.2012.02.011

Lin, W., Faure, M., Monie, P., Scharer, U., Zhang, L. S., and Sun, Y. (2000). Tectonics of SE China: new insights from the lushan massif (jiangxi province). *Tectonics* 19, 852–871. doi:10.1029/2000tc900009

Liu, C., Li, G., and Liu, F. (2022). Early Cretaceous-Cenozoic exhumation history of luxi terrane and adjacent areas, eastern North China craton. *Geol. J.* 57, 2735–2748. doi:10.1002/gj.4445

Liu, F., Yang, F., Zheng, D., Ding, H., Li, C., and Jepson, G. (2024). Apatite (U-Th)/He thermochronological constraints on the landscape evolution linked to the normal faulting in taishan Mountain, Eastern China. *Lithosphere* 279, 21. doi:10.2113/2023/lithosphere_2023_279

Liu, Q. Y., He, L. J., and Huang, F. (2013). Review of Mesozoic geodynamics research of South China. *Prog. Geophys*, 28 (2), 633–647. (in Chinese with English abstract). doi:10.6038/pg20130212

Liu, S. C., Xia, Q. K., Choi, S. H., Deloule, E., Li, P., and Liu, J. (2016). Continuous supply of recycled Pacific oceanic materials in the source of Cenozoic basalts in SE China: the Zhejiang case. *Contributions Mineralogy Petrology* 171, 100–131. doi:10.1007/s00410-016-1310-4

Lu, L. L., Jiang, S. H., Li, S. Z., Wang, P., Jiang, Y., Wang, G., et al. (2022). Evolution of meso-cenozoic subduction zones in the ocean-continent connection zone of the eastern South China Block: insights from gravity and magnetic anomalies. *Gondwana Res.* 102, 151–166. doi:10.1016/j.gr.2020.12.010

Ludwig, K. (1991). *ISOPLOT: a plotting and regression program for radiogenic-isotope data, version 2.53*. Reston, Virginia, USA: U.S. Geological Survey Open File Report. 91-445.

Meng, L. F., Li, Z. X., Chen, H. L., Li, X. H., and Wang, X. C. (2012). Geochronological and geochemical results from Mesozoic basalts in southern South China block support the flat-slab subduction model. *Lithosphere* 132-133, 127–140. doi:10.1016/j.lithos.2011.11.022

Peng, B. X., Wang, Y. J., Fan, W. M., Peng, T. P., and Liang, X. Q. (2006). LA-ICP-MS zircon U-Pb dating for three Indosinian granitic plutons from central Hunan and western Guangdong provinces and its petrogenetic implications. *Acta Geol. Sinica-English Ed.* 80 (5), 660–669. doi:10.1111/j.1755-6724.2006.tb00290.x

Reiners, P. W., Spell, T. L., Nicolescu, S., and Zanetti, K. A. (2004). Zircon (U-Th)/He thermochronometry: he diffusion and comparisons with $^{40}Ar/^{39}Ar$ dating. *Geochimica Cosmochimica Acta* 68 (8), 1857–1887. doi:10.1016/j.gca.2003.10.021

Shi, H. C., Shi, X., Glasmacher, U. A., Yang, X. Q., and Stockli, D. F. (2016). The evolution of eastern sichuan basin, yangtze block since Cretaceous: constraints from low temperature thermochronology. *J. Asian Earth Sci.* 116, 208–221. doi:10.1016/j.jseaes.2015.11.008

Shi, X. B., Kohn, B., Spencer, S., Guo, X. W., Li, Y. M., Yang, X. Q., et al. (2011). Cenozoic denudation history of southern Hainan island, South China Sea: constraints from low temperature thermochronology. *Tectonophysics* 504, 100–115. doi:10.1016/j.tecto.2011.03.007

Shi, X. B., Kohn, B., Yu, C. H., Tian, Y. T., Li, G. W., and Zhao, P. (2022). Thermo-tectonic history of coastal NW South China Sea: a low-temperature thermochronology study. *Tectonophysics* 833, 229344. doi:10.1016/j.tecto.2022.229344

Shu, L. S., Zhou, X. M., Deng, P., Wang, B., Jiang, S. Y., Yu, J. H., et al. (2009). Mesozoic tectonic evolution of the Southeast China block: new insights from basin analysis. *J. Asian Earth Sci.* 34, 376–391. doi:10.1016/j.jseaes.2008.06.004

Sibuet, J. C., Hsu, S. K., Pichon, X. L., Formal, J. P., Reed, D., Moore, G., et al. (2002). East Asia plate tectonics since 15 ma: constraints from the Taiwan region. *Tectonophysics* 344, 103–134. doi:10.1016/s0040-1951(01)00202-5

Suo, Y. H., Li, S. Z., Jin, C., Zhang, Y., Zhou, J., Li, X. Y., et al. (2019). Eastward tectonic migration and transition of the Jurassic-cretaceous Andean-type continental margin along southeast China. *Earth-Science Rev.* 196, 102884. doi:10.1016/j.earscirev.2019.102884

Tao, N., Li, Z. X., Martin, D., Evans, N. J., Li, R. X., Pang, C. J., et al. (2019). Post-250 Ma thermal evolution of the central Cathaysia block (SE China) in response to flat-slab subduction at the proto-Western Pacific margin. *Gondwana Res.* 75, 1–15. doi:10.1016/j.gr.2019.03.019

Tao, N., Li, Z. X., Martin, D., Noreen, J. E., Geoffrey, E. B., Li, W. X., et al. (2017). Thermochronological record of middle–late Jurassic magmatic reheating to Eocene rift-related rapid cooling in the SE South China block. *Gondwana Res.* 46, 191–203. doi:10.1016/j.gr.2017.03.003

Tian, M. Y., and Di, Y. J. (2024). Petrogenesis of Jurassic granitic rocks in south China block: implications for events related to subduction of Paleo-Pacific plate. *Petrogenesis Jurass. granitic rocks South China Block Implic. events Relat. subduction Paleo-Pacific plate. Geosciences* 16, 20220601. doi:10.1515/geo-2022-0601

Tian, M. Y., and Di, Y. J. (2025). Geochronology, petrogeochemistry, and geodynamic processes affecting the Indosinian granitic rocks in South China: a review. *Geochronol. petrogeochemistry, Geodyn. Process. Affect. Indosinian granitic rocks South China a Rev. Int. J. Earth Sci.* 114, 445–465. doi:10.1007/s00531-025-02505-2

Vermeesch, P. (2009). RadialPlotter: a java application for fission track, luminescence and other radial plots. *Radiat. Meas.* 44 (4), 409–410. doi:10.1016/j.radmeas.2009.05.003

Wang, X. Y., Suo, Y. H., Li, S. Z., Cao, X. Z., Li, X. Y., Zhou, J., et al. (2020a). Cenozoic uplift history and its dynamic mechanism along the eastern continental margin of South China. *Acta Petrol. Sin.* 36 (6), 1803–1820. doi:10.18654/1000-0569/2020.06.10

Wang, Y., Wang, Y. J., Li, S. B., Seagran, E., Zhang, Y. Z., Zhang, P. Z., et al. (2020b). Exhumation and landscape evolution in eastern South China since the Cretaceous: new insights from fission-track thermochronology. *J. Asian Earth Sci.* 191, 104239. doi:10.1016/j.jseaes.2020.104239

Wang, Y. J., Fan, W. M., Zhang, G. W., and Zhang, Y. H. (2013). Phanerozoic tectonics of the South China block: key observations and controversies. *Gondwana Res.* 23, 1273–1305. doi:10.1016/j.gr.2012.02.019

Xiao, W. Z., Zi, F., Zhang, C. G., Xie, F. Q., Sanislav, I. V., Fnais, M. S., et al. (2024). Long-lasting magmatic, metamorphic events in the Cathaysia block: insights from the geochronology and geochemistry of inherited zircons in Jurassic A-Type granites. *Minerals* 14 (12), 1247. doi:10.3390/min14121247

Yan, B., Li, W. X., Huang, X. L., Yu, Y., and Tao, J. H. (2024). An anomalous rollback process of Mesozoic flat-slab subduction in South China. *An anomalous roll back process Mesoz. flat-slab subduction South China. Tectonophys.* 874, 230252. doi:10.1016/j.tecto.2024.230252

Yan, Y., Carter, A., Xia, B., Ge, L., Brichau, S., and Xiaoqiong, H. (2009). A fission track and (U-Th)/He thermochronometric study of the northern margin of the south China Sea: an example of a complex passive margin. *Tectonophysics* 474, 584–594. doi:10.1016/j.tecto.2009.04.030

Yu, J. H., O'Reilly, S. Y., Wang, L. J., Griffin, W. L., Zhou, M. F., Zhang, M., et al. (2010). Components and episodic growth of Precambrian crust in the Cathaysia block, south China: evidence from U–Pb ages and Hf isotopes of zircons in Neoproterozoic sediments. *Precambrian Res.* 181, 97–114. doi:10.1016/j.precamres.2010.05.016

Yue, Y. F., Xia, X. P., Li, P., He, B., Peng, T., Sun, M., et al. (2024). Revisiting the high temperature darongshan-shiwandashan granitoids in the South China: a response to slab tearing associated with diachronous collision between indochina and South China blocks. *Revisiting high Temp. Darongshan-Shiwandashan granitoids South China a response slab tearing Assoc. diachronous Collis. between Indoch. South China blocks. Lithos* 494–495, 107898. doi:10.1016/j.lithos.2024.107898

Zeng, G., He, Z. Y., Li, Z., Xu, X. S., and Chen, L. H. (2016). Geodynamics of paleo-pacific plate subduction constrained by the source lithologies of late Mesozoic basalts in southeastern China. *Geophys. Res. Lett.* 43, 10189–10197. doi:10.1002/2016gl070346

Zhang, G. P. (2007). *The uplift process research of pluton in Mesozoic in Guangdong province [Ph.D. thesis]*. Changshan: Central South University. (in Chinese with English abstract).

Zhang, G. W., Guo, A. L., Wang, Y. J., Li, S. Z., Dong, Y. P., Liu, S. F., et al. (2013). Tectonics of south China continent and its implications. *Sci. China Earth Sci.* 56 (11), 1804–1828. doi:10.1007/s11430-013-4679-1

Zhang, Z. J., and Wang, Y. H. (2007). Crustal structure and contact relationship revealed from deep seismic sounding data in south China. *Phys. Earth Planet. Interiors* 165 (1), 114–126. doi:10.1016/j.pepi.2007.08.005

Zhao, P., Shi, X. B., Liu, L., Liu, K., Shen, Y. Q., Ren, Z. Q., et al. (2025). A late Paleogene erosion event in the sanshui basin, southern margin of the south China block and its tectonic significance. *Tectonophysics* 894, 230557. doi:10.1016/j.tecto.2024.230557

Zheng, C., Xu, C. H., Manfred, R. B., and Zhou, Z. (2019). Evolution and provenance of the xuefeng intracontinental tectonic system in south China: constraints from detrital zircon fission track thermochronology. *J. Asian Earth Sci.* 176, 264–273. doi:10.1016/j.jseaes.2019.02.012

Zhou, D., Ru, K., and Chen, H. Z. (1995). Kinematics of Cenozoic extension on the South China Sea continental margin and its implications for the tectonic evolution of the region. *Tectonophysics* 251, 161–177. doi:10.1016/0040-1951(95)00018-6

Zhou, X. M., and Li, W. X. (2000). Origin of late Mesozoic igneous rocks in Southeastern China: implications for lithosphere subduction and underplating of mafic magmas. *Tectonophysics* 326 (3), 269–287. doi:10.1016/s0040-1951(00)00120-7

Zhou, X. M., Sun, T., Shen, W. Z., Shu, L. S., and Niu, Y. L. (2006). Petrogenesis of Mesozoic granitoids and volcanic rocks in South China: a response to tectonic evolution. *Episodes* 29, 26–33. doi:10.18814/epiiugs/2006/v29i1/004